Cable and Motor Winding Impedance Interactions in Motor Drive Systems and its Impact on HF Overvoltages

Yalda Azadeh, *Graduate Student Member, IEEE*, Kushan Choksi, *Graduate Student Member, IEEE*, Abdul Basit Mirza, *Graduate Student Member, IEEE*, Xiaolong Zhang, *Member, IEEE*, Yuxuan Wu, *Graduate Student Member, IEEE*, Fang Luo, *Senior Member, IEEE*, and Kiruba S. Haran, *Fellow, IEEE*

***Abstract*—Voltage stress across motor winding is critical for insulation health when its series resonance frequencies, which have the least impedances, known as antiresonances, coincide with overvoltage (OV) resonance frequencies across it, named as antiresonance phenomenon (ARP). First, this article discloses that the OV resonance frequencies across motor winding (load) can be represented by the combination impedance of cable plus load. Second, it investigates the interactions between the cable and load impedances in different layouts and examines their impact on the ARP. Then, it discloses the sensitivity of ARP versus cable and load impedance parameters. Lastly, the ARP's correlation with these parameters establishes a safe operation area as a motor drive system design guideline. Contrary to the general belief that systems using short cable or integrated systems have less insulation damage, this study shows that the OV stress in these systems can be critical. This article offers a simplified methodology to optimize the reliability of the drive system and mitigate the ARP. By using this approach, the article suggests that the time-consuming iterative design of *dV/dt* filters or overdesign of insulation can be eliminated. The practical test and modeled system are conducted to validate the approach.**

***Index Terms*—Antiresonance phenomenon, impedance interactions, overvoltages, PWM-based motor drive system reliability, safe operation area, voltage stress.**

I. Introduction

THE emerging application of wide band gap (WBG) devices in motor drive systems brings higher *dV/dt* to the system [1] and [2], while the new generation design of high-power density motor drives with low winding impedance is growing [3]. Combining these factors brings interactions among different parts of the system and higher challenges in insulation design [4]. The transient voltages caused by traveling waves through the cable between the inverter and the motor can cause higher motor side overvoltages (OVs), referred to as reflected wave phenomenon (RWP) ([4], [5], and [6]), causing insulation and reliability issues which ultimately cause the failure of the motor drive system [7]. However, characterizing this high-frequency phenomenon is complex owing to increased dV/dt and the complex network of the resonance circuits in motor drives, see Fig. 1.

While knowledge of the OV magnitude is important, it is not sufficient to ensure the reliability of the motor winding. Voltage stress across insulation directly relates to the value of overvoltage over the impedance magnitude (|overvoltage/impedance|) [10]. The voltage stress across motor winding poses a risk to the insulation reliability if the OV resonance frequency coincides with the frequency of its differential mode (DM) impedance antiresonance (higher-leakage current through insulation). This phenomenon is called the antiresonance phenomenon (ARP), and the frequency band is termed antiresonance (AR) frequency [10], as shown in Fig. 2.

To provide a clearer explanation of the ARP occurrence, Fig. 2 displays a sample of a fast Fourier transform (FFT) of the OV waveform across load versus frequency response of load DM impedance waveform in a WBG-based drive system. These waveforms are gained from the experimental practice in this study, which will be further elaborated in Section IV.

The red waveform shows the OV resonances across the load terminal measured from the terminal BB' shown in Fig. 1. Terminal B is the power line, and terminal B' is the phase b and c as the return line in this measurement. So, this OV resonance includes the resonance networks of the drive system, including cable+ load (not only load) across the load. This resonance network shows three peaks, as in Fig. 2. On the other hand, the blue waveform in Fig. 2 is gained from the differential mode impedance measured only across the load.

By superimposition of the OV resonances of the drive system with the load impedance in the frequency domain, it is seen that only the third resonance of the OV resonances coincides with the impedance antiresonance. The first and second resonances are away from the impedance AR frequency with a good margin. This shows that the voltage stress could still be

Manuscript received 24 April 2023; revised 23 August 2023; accepted 29 September 2023. Date of publication 6 October 2023; date of current version 6 December 2023. This work was supported by the U.S. Federal Aviation Administration and NSF under Grants 692M15-20-C-00010 and 1846917. Recommended for publication by Associate Editor D. Dujic. *(Corresponding author: Yalda Azadeh.)*

Yalda Azadeh, Kushan Choksi, Abdul Basit Mirza, Yuxuan Wu, and Fang Luo are with the Electrical and Computer Engineering Department, Stony Brook University, Stony Brook, NY 11794 USA (e-mail: yalda.azadeh@stonybrook.edu; choksi.kushan@stonybrook.edu; abdulbasit.mirza@stonybrook.edu; yuxuan.wu@stonybrook.edu; fang.luo@stonybrook.edu).

Xiaolong Zhang and Kiruba S. Haran are with the Electrical and Computer Engineering Department, University of Illinois at Urbana Campaign, Champaign, IL 61820 USA (e-mail: xzhng157@illinois.edu; kharan@illinois.edu).

Color versions of one or more figures in this article are available at https://doi.org/10.1109/TPEL.2023.3322639.

Digital Object Identifier 10.1109/TPEL.2023.3322639

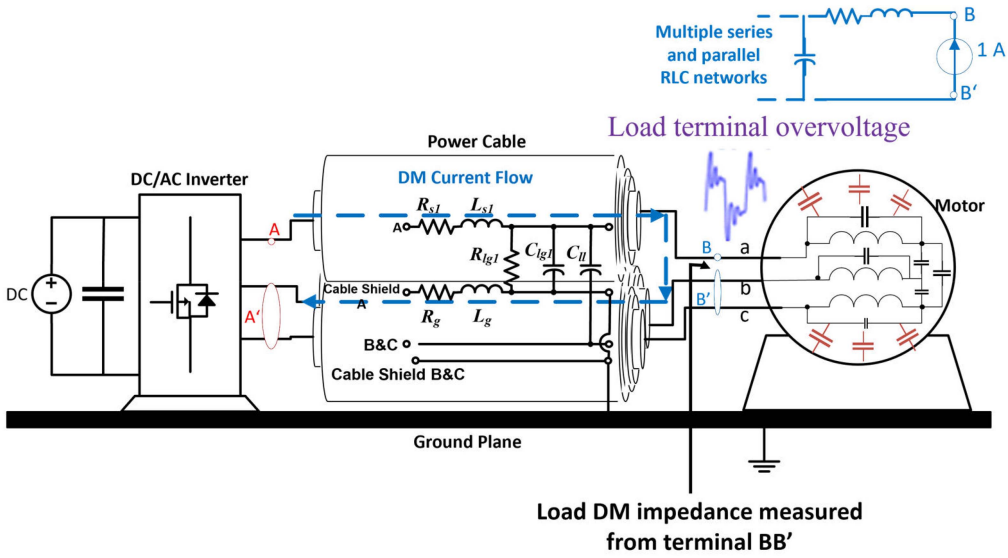

Fig. 1. Cable-connected motor drive system schematic.

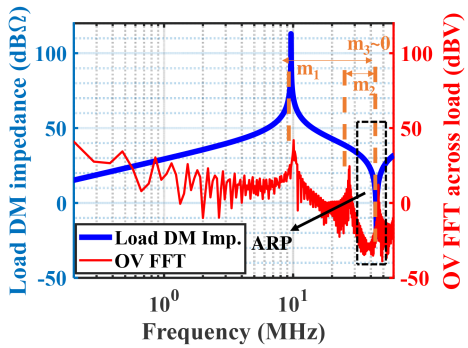

Fig. 2. Introduction to ARP occurrence.

critical even for secondary resonances, although having lower OV magnitude. So, the secondary OV resonances that coincide with the AR of the load must also be mitigated. Interestingly, previous works [8], [9], and [11] have mainly focused on investigating and alleviating only the primary OV resonance frequencies in a motor drive system. This also highlights the importance of this study in alleviating secondary resonances causing ARP.

Furthermore, it is known that long cables always cause critical OV across the load, while motor drives with shorter cables are less susceptible to this issue [12]. However, it is shown in this article that even with shorter cables, the ARP can happen. Moreover, the integrated drive system is bound to the ARP occurrence. So, the voltage stress across the motor winding could still be significant and detrimental.

The occurrence of ARP is dependent on the motor drive resonance networks, i.e., resonances of cable+ load DM impedance and load DM impedance AR [10]. Hence, prediction of the OV resonance frequencies is necessary versus the different configuration and layout of the system.

In [9] and [11], the empirical study is exploited to extract the OV resonance frequencies with varying cable lengths and system impedance parameters in different cases. So, testing different layouts, conducting modeling, and testing repeatedly to achieve the optimum system design would indeed be time-consuming and require additional tools and effort.

In [10], [13] and [14], the OV resonance frequency across the load is exploited to follow $1/4l_c\tau_p$ equation in systems with longer cables, which l_c and τ_p are the cable length and propagation delay, respectively. The equation is applicable regardless of the load characteristic. In the specific drive system under study in [10], the longer cable resonant network dominates over the load, causing the OV. However, this equation is not valid for the short cable due to the contribution of load parasitics in the OV resonances. Furthermore, such an equation does not provide secondary resonance frequencies. Thus, a comprehensive theory is still required to cover different system configurations to understand all the resonance frequencies of the overvoltage.

The AC small-signal modeling of the system would give more generic OV information [15]. However, the modeling would be very complicated for high-order LC networks.

Frequency domain impedance-based analysis with direct impedance measurement can be more straightforward in identifying the OV resonance frequencies. In [16], cable+ load impedance measured from the converter terminal as terminal AA' shown in Fig. 1, is not representative of the OV resonance frequencies using cables of different lengths. It is shown in Section IV that the impedance response that accurately determines the OV resonance frequencies should be measured from the OV point of study, terminal BB' shown in Fig. 1.

Furthermore, bulky and costly sine wave or dV/dt filters [17] or thickening the insulation is suggested by traditional voltage stress mitigation approaches to mitigate ARP [17]. However, this reduces the benefits of employing WBG devices. Moreover, as the ARP is subject to system layout variation [9], filter/ insulation design would require modification/ change with varying cabling/ load configuration and electric layout.

Therefore, it is paramount to understand ARP sensitivity to such configuration/ layout and look for a solution to incorporate into the system design and layout for the safe operation of the system.

To address the mentioned research gaps, the motivation is to 1) appropriately measure the combination impedance of cable+ load, which represents the OV high frequency (HF) resonances across the load. 2) Investigate the cable and load HF impedance interaction in different layouts, which causes ARP. 3) Then, safe operation area (SOA) away from the ARP across load can be defined by knowledge of ARP occurrence versus different impedance parameters.

1) The impedance-based method of investigation of the ARP in a motor drive system would be faster/simpler, and more accurate compared to literature [9], [10], [11] and [13], [14], [15], [16]
2) As the impedance-based approach is independent of the type of configuration/ layout, it is extendable on different cabling/ load configurations and electric layouts.
3) Revisits the drive system configuration and layout based on the ARP occurrence.
4) Secondary reliability solutions like filter design or overdesign of the insulations can be eliminated using the modeling to do sensitivity analysis to mitigate the ARP versus parameters variation. So, it would also provide a high-power density solution.

In the following sections, first, the system under test and the impedance parameters involved in this study are introduced and modeled. The modeling is validated through experimental results. After that, the ARP occurrence is investigated versus cable and load impedance parameters representing different system configurations/layouts. Finally, the ARP sensitivity analysis versus impedance parameters is given in driving an SOA for a motor drive system to mitigate ARP.

II. Literature Review on Motor Drive System Modeling and Impedance Characterization

In this paper, the motor drive system is modeled using published works [18], [19], [20], [21], [22], [23] and briefly described here to (1) introduce the impedance parameters of the system under study, (2) use this modeling to give guideline to do ARP sensitivity analysis and gain a cable/ motor winding SOA mitigating ARP afterward; where you could design the system or optimize the layout for a reliable motor drive system operation.

Cable and motor-winding in WBG motor drives are attribute to high-frequency noise, owing to impedance mismatch OVs, high-frequency mutual coupling, skin effect [16], and proximity effect [24]. These parasitic elements are layout and length-dependent. So, modeling requires to be adaptable with system configuration and extendable for HF.

A. HF Cable Modeling

Length extendibility and infrastructural robustness (accommodating all parasitic elements of cabling) of cable modeling are paramount for accurate modeling of ARP. This can be achieved by rigorous cable impedance characterization and RWP experiments using a double pulse test (DPT). The methodology of cable modeling is presented in detail in [18], which explains a sequential and hybrid simulation-experiments approach. It uses R-L and R-C ladders to represent skin and proximity effects, respectively, as suggested in Fig. 3(a). Parasitic extraction can be divided into self, common mode (CM), and DM impedance measurements. The extraction equations are as suggested in [18]. The self-experiments extract cable inductance and resistance as L_{s1}, R_{s1} and mutual coupling. The skin inductance and resistance defined as L_{s2}, R_{s2} lead to increased resistance at HF extracted from DM experiments [18]. R_g and L_g refer to ground resistance and inductance, respectively. It can be used to model variation in the type of shield or grounding technique. R_{ll1}, R_{ll2}, C_{ll1} and C_{ll2} refer to parasitic resistance and capacitance between the cables (line to line).

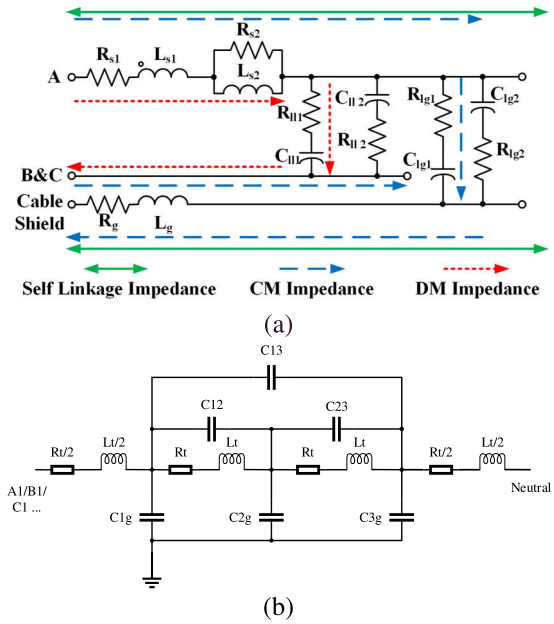

Fig. 3. High-frequency model (a) cable (b) coil.

It should be noted R_{ll1}, R_{ll2}, C_{ll1} and C_{ll2} effectively form a ladder circuit, which can be used to model proximity effect high-frequency behavior between the cables. They can be extracted using DM open circuit impedance measurement. Also, parasitic C_{lg1}, C_{lg2}, R_{lg1}, and R_{lg2} are phase-to-ground parasitic extracted from CM open circuit impedance analysis incorporating proximity effect changes [18]. It should be mentioned that the lumped model of LC networks for the 1 m per unit cable length was accurate enough in this paper to be representative of the practical layout, which is shown in Section III.

B. HF Coil Modeling

The HF model for a form wound coil under test is an impedance network of nodes connected by inductive, resistive, individual turns in the coil. Fig. 3(b) shows a network model for a three-turn coil. Lt, Rt, Cij, and Cig represent inductance

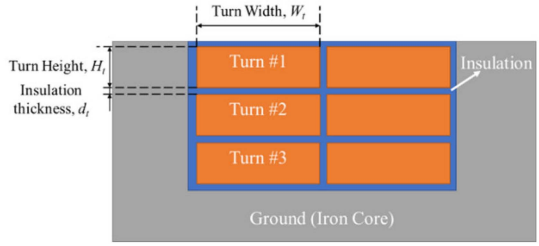

Fig. 4. Machine slot structure.

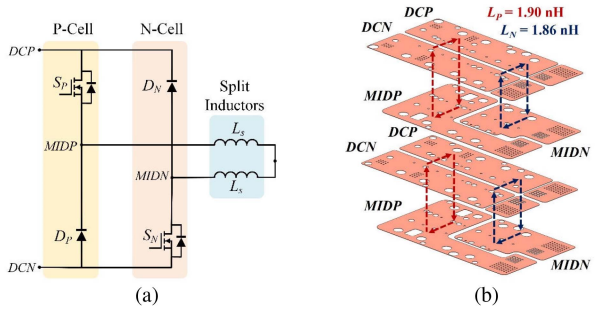

Fig. 5. (a) Split-phase converter schematic (b) exploded view of developed PCB layout (four layers) [23].

per turn, the resistance per turn, the capacitance between any two turns, and the capacitance between turn and ground, respectively. The network can be extended by adding more nodes and associated elements to incorporate more turns or multiple phases. Turn inductance is a lumped parameter that includes both self-inductance and turn-turn mutual inductance. Analytical determination of the parameters is given as follows.

In Fig. 4, a machine slot structure with a three-turn coil sitting inside it is shown. One turn's width, height, and axial length are W_t, H_t, and l_t, respectively. This geometry will be used as an example to determine the parameters in Fig. 3(b).

Turn dc resistance is determined by Ohm's Law, i.e.,

$$R_{DC} = \frac{l_t}{\sigma_c k_{fil} W_t H_t} \tag{1}$$

where σ_c is the copper conductivity and k_{fil} is the copper fill factor. However, the turn resistance increases with the excitation frequency due to skin and proximity effects. A resistance factor is introduced:

$$R_t = k_R R_{DC} \tag{2}$$

At high frequencies, k_R is approximately [21]

$$k_R \approx \frac{2z_t^2 + 1}{3}\xi \tag{3}$$

where z_t is the number of turns, and ξ is the reduced conductor height, defined as

$$\xi \approx H_t \sqrt{\frac{1}{2}\omega\mu_0\sigma_c \frac{2W_t}{W_s}} \tag{4}$$

where ω is the electrical frequency, μ_0 is void permeability, and W_s is the slot width.

Turn inductance consists of two parts, i.e., self-inductance and turn-turn mutual inductance. They need to be found by solving the magnetic circuit either analytically or through finite element (FE) modeling methods. For the test setup where no iron core is used, the inductance is obtained from a magnetostatic FE model. For the slotted structure, a simple magnetic circuit analysis gives the self-inductance as

$$L_t = \frac{\mu_0 \tau_p l_t}{k_c g} + L_\sigma \tag{5}$$

where τ_p is pole pitch (circumferential distance between both sides of one coil), g is the airgap length, k_c is Carter's coefficient, and L_σ is the leakage inductance. Turn-turn mutual inductance within one phase is given as

$$M_t = \frac{\mu_0 \tau_p l_t}{k_c g} \tag{6}$$

The capacitance between two conductors is determined by their distance and the dielectric constant of the insulation material. For example, the parasitic capacitance between Turn #1 and Turn #2 can be calculated as

$$C_{12} = \frac{\varepsilon_r \varepsilon_0 W_t l_t}{d_t} \tag{7}$$

where ε_r and d_t are the dielectric constant and thickness of the insulation material, ε_0 is the vacuum permittivity. The expressions for other capacitive elements can be derived in a similar way [21].

C. HF Converter Modeling

The converter used for this study is a split-phase leg comprising P and N-cells, with split inductors L_s connecting the midpoints of both cells (Fig. 5(a) [22] and [23]. For the study, the split inductors are omitted from the circuit and DPT is performed with the N-cell only, with cable and load connected across the diode D_N.

The split-phase leg is built using SiC MOSFET C3M0016120 from Cree and SiC Schottky Diode FFSH50120A from Onsemi. Both devices are in TO-247 packages with a lead inductance of approximately 7 nH per leg [22]. Fig. 5(b) shows the designed PCB layout with a vertical power loop layout. Due to the high current carrying requirement, two layers are allocated for each node, resulting in a four-layer PCB with 3 oz copper per layer. The inductance L_{PCB} is extracted using ANSYS Q3D solver with a solver frequency of 100 MHz. The total power loop inductance L_{LOOP} hence, is a sum of PCB and device lead inductance, which comes out to be approximately $L_{LOOP} = L_{PCB} + 4\,L_{PAK} = 30$ nH for both P and N-Cells.

The value of L_{LOOP} is negligible compared to the cable and motor winding impedance parameters in such a case study [25]. So, their impact on the OVs' resonance frequency and magnitude is negligible in this paper.

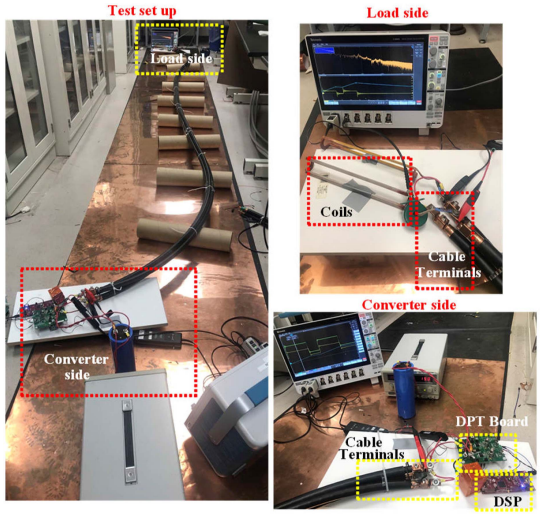

Fig. 6. RFW DPT setup.

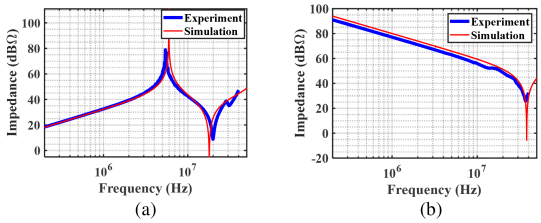

Fig. 7. Impedance matching of experimental measurement vs. modeled cable+ load using 1 m cable. (a) DM. (b) CM.

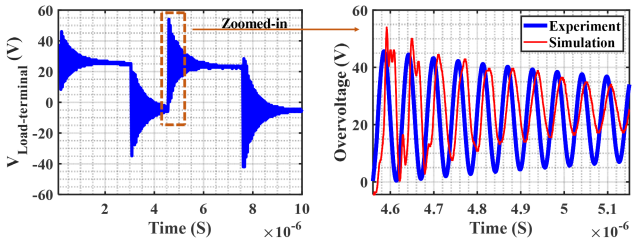

Fig. 8. RFW results matching in practical and simulation DPT at load terminal using 1 m cable.

III. Impedance Model Validation

In this section, the drive system modeling is validated through experimental results. Coils are used as the sample of motor winding load to represent a low-impedance motor winding with HF impedance interactions in a motor drive system. The cables and load are set up in the same testbed for impedance measurements as for DPT, shown in Fig. 6.

The CM and DM modeled impedance for cable only, coil (load) only, and combination impedance of cable and coil (cable+ load) is superimposed with the experimental measurement results using 1 and 6 m cables. The cable+ load impedance superimposition is given in Fig. 7 for the system using 1 m cable, which shows a close match. The test is conducted for various voltage levels. Fig. 8 shows the load terminal voltage waveforms superimposed in frequency and amplitude in simulation and practical DPT using a 1 m cable. The DPT using long cable is similarly modeled by cascading the modeled networks for cable and validation, which is out of the scope of this article.

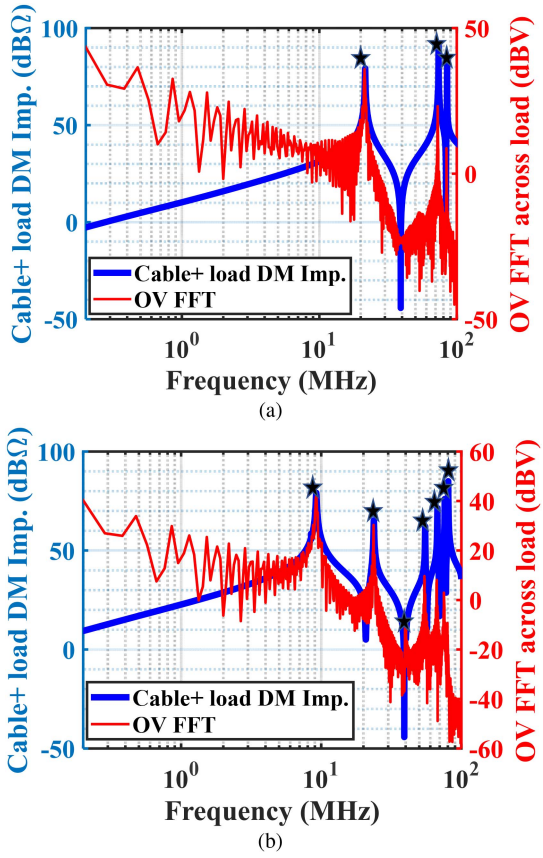

Fig. 9. Prediction of the OV resonance frequencies across load by impedance measurement at terminal BB' using (a) 1 m and (b) 6 m cable.

IV. Motor Winding Terminal HF OV Stress and Its Mitigation

A. Motor Winding Terminal High-Frequency OV Prediction

The accurate prediction of the OV resonance frequencies is required to mitigate ARP in the design or layout step. Therefore, in this article, an accurate and fast way, impedance-based prediction, is proposed. The measurement is extendable to different cabling/ load types and electric layouts.

The voltage between any two nodes is related to impedance characteristics between those nodes [26]. Hence, to estimate OV resonance frequencies across the load by impedance analysis, the cable+ load impedance should be measured across its terminal, BB' shown in Fig. 1.

Cable+ load DM impedance measured across the load terminal is given in Fig. 9 versus the FFT of the OV waveform across the load terminal using 1 and 6 m cables. The OV comprises frequency components that match the parallel resonances' frequency in cable+ load DM, marked by stars in the figure. Thus, with off-line impedance measurement of cable+ load, its resonance frequencies represent the OV resonances across a

load. This can be very helpful for system debugging as well as modeling.

The proposed method is simpler and faster compared to empirical and modeling-based extraction of the OV resonance frequencies in [9], [10] and [18]. It saves two steps in gaining the resonance frequencies: (1) performing continuous/DPT test, and (2) accurate high measurement for post-processing (FFT). This benefit is highlighted when (1) the system is too complex to model, (2) in empirical-based prediction methods, as the presented approach bypasses rigorous efforts and elements/tools for modeling/testing.

Furthermore, the proposed approach is extendable on different cabling/ load configurations and electric layouts as it is independent of type of the system and only needs measurement from the point of interest in the OV study.

It is demonstrated that the OV resonance frequencies can be predicted by only impedance-based measurements, so it is also possible to predict the ARP of the motor drive system shown in the following section.

B. Motor Winding Terminal ARP Prediction

In this paper, two kinds of segregated and integrated motor drive systems are under study to provide a comprehensive vision of the ARP occurrence. The cable+ load measured impedance across the load terminal, representing the OV resonance frequencies, in a segregated system (using 1 and 5 m cable) and an integrated drive system (without cable), is shown in the same frame with DM impedance frequency sweep of the load.

1) Segregated Motor Drive System: In this section, the ARP is under study for the motor drive system using 1 and 5 m cables. The ARP occurrence possibility is shown in Fig. 10, with the margin from coinciding the AR of load DM impedance with parallel resonances of cable+ load impedance across the load, "m." For more validation, the load DM impedance is also shown versus OV FFT across load in Fig. 11. It can be seen that because of the impedance-based prediction of the OV resonance frequencies presented in the previous section, Figs. 10 and 11 provide the same information about the ARP occurrence.

As can be seen from Figs. 10 and 11(a), the OV frequencies are away from the AR using a 1 m cable. However, the third OV resonance happens at the same frequency as the load DM impedance AR using 5 m cable at 43 MHz, as shown in Figs. 10 and 11(b). Therefore, there is a requirement to mitigate the ARP using a 5 m cable as the case study here.

It should be noted that not only the high amplitude OV resonances need to be mitigated, but also the less amplitude OV resonances at the frequencies in which ARP happens have importance to be mitigated. Moreover, in the case of filter design, secondary OV resonances would also be of great importance to be filtered out. So, by understanding the ARP with different cabling/ load configurations and electric layout, such an impedance interaction should be mitigated.

In the following, the initial discussion and guideline are given on mitigation/ optimization of such kinds of the ARP. Two solutions can be implemented in the case study with a 5 m cable,

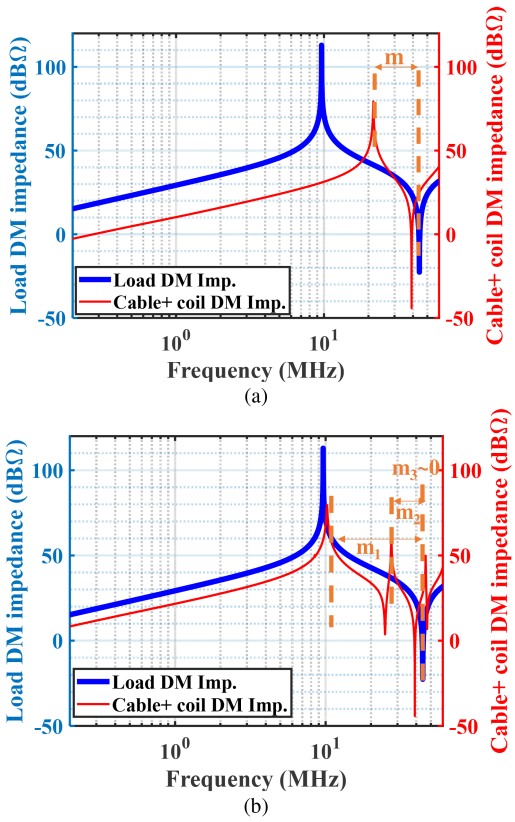

Fig. 10. Cable and motor winding interactions and margin from ARP using (a) 1 m and (b) 5 m cable.

either to shift the OV to the higher or lower frequency away from the ARP.

To move the OV to the higher frequency, one way would be to decrease the length of the cable to a shorter value [13] to shift them away from the load antiresonance frequency, which may not be practical in specific applications. Using the other solution, to shift the OV to a higher frequency by putting a filter capacitance at the motor side [8], the antiresonance of the load side also would shift and needs to reassess the impedance characteristics.

Using an inductive filter or increasing the length are some ways to shift the OV to the lower frequencies. By increasing the length of the cable, the safety margin for the higher amplitude OV resonance, shown as m_1, increases and mitigates the worst-case scenario. However, due to the several networks of the resonance circuits in a motor drive system, the secondary OV ringing shows up. Still, due to the secondary-OV frequencies, the ARP happens, as shown in Figs. 10 and 11(b). Other approaches to mitigation of the ARP are investigated by conducting the ARP sensitivity study versus impedance parameters in section C.

2) Integrated Motor Drive System: Integrated motor drives gain more popularity where space is a primary concern [27]. It is mentioned in previous works that the OV, due to the long cable between the motor and the inverter, can be eliminated with an integrated drive system [12]. However, it is shown in this paper that due to the ARP, the underlying OV stress across motor

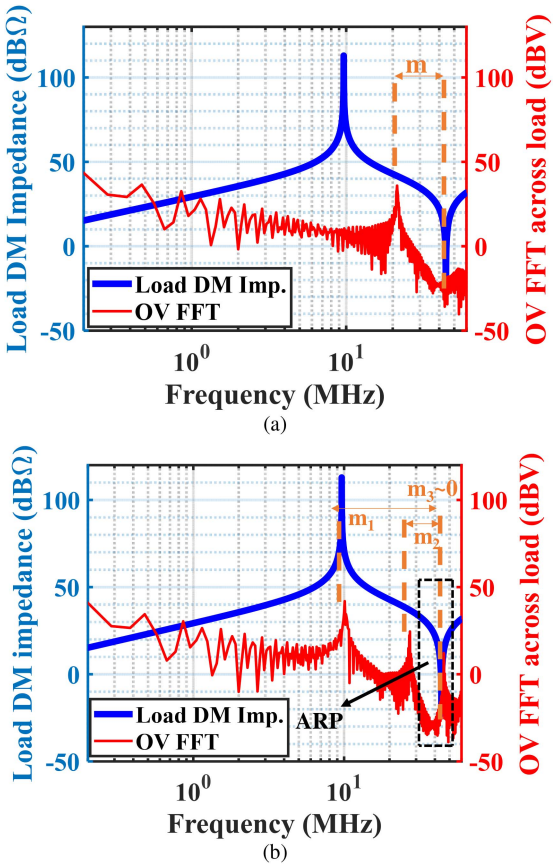

Fig. 11. Cable and motor winding interactions and margin from ARP using (a) 1 m and (b) 5 m cable.

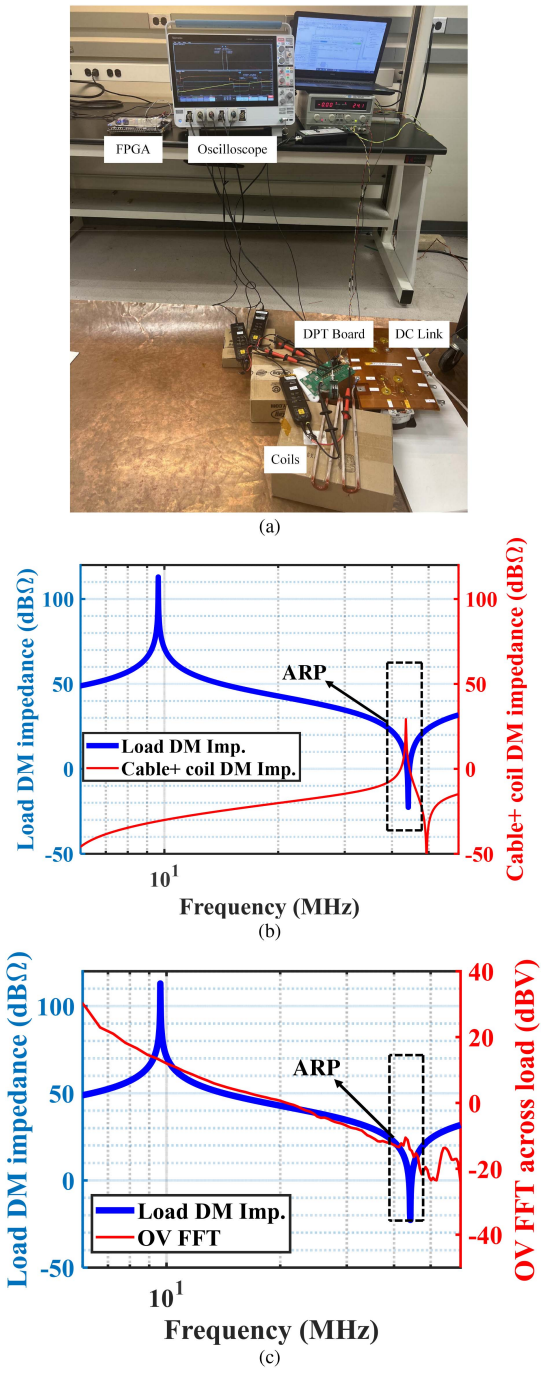

Fig. 12. Integrated motor drive (a) DPT setup; ARP given for (b) load impedance versus cable+ load impedance and (c) load impedance versus OV FFT across a load.

winding can become excessive. A lack of clear understanding of the OV could cause insulation degradation of the motor winding.

The DPT test setup shown in Fig. 12(a) is used to study ARP in an integrated motor drive system as a guideline. The load is connected directly to the DPT converter without any cable in between. It should be noted that excitation amplitude is kept the same for the segregated and integrated case studies. As is shown in Fig. 12(b) and (c), although the amplitude of the OV resonance is lower in the integrated system compared to the segregated drive system, it aligns with the load DM impedance AR frequency. It should be highlighted that an integrated drive system is always bound to the occurrence of ARP. Because of the absence of cable, the OV resonance frequency across the load terminal is the same as the load antiresonance frequency. Hence, the voltage stress across the load becomes critical and requires mitigation.

In conclusion, in section B, it is demonstrated that the voltage stress is not solely determined by cable length. The ARP can happen,depending on the cabling/ load impedance interactions. In addition to the primary resonances that cause ARP, the secondary resonances can be equally damaging. So, it requires mitigation in the case of ARP occurrence.

As discussed in section B, the length of the cable is one freedom degree to optimize the design reliability according to the application. However, if the design is limited by some regulations that do not allow to selection of the solutions given, varying other impedance parameters could give the required margin away from ARP. So, this observation gives a good reason to study the impedance interactions between different parameters of the cable and motor winding and their influence on ARP. So, in the following, the sensitivity of the ARP across motor winding in regard to different impedance parameters is exploited for the given system in this article. This would give a good pathway to study the system under test to optimize a reliable motor drive system operation in regards to mitigating the ARP.

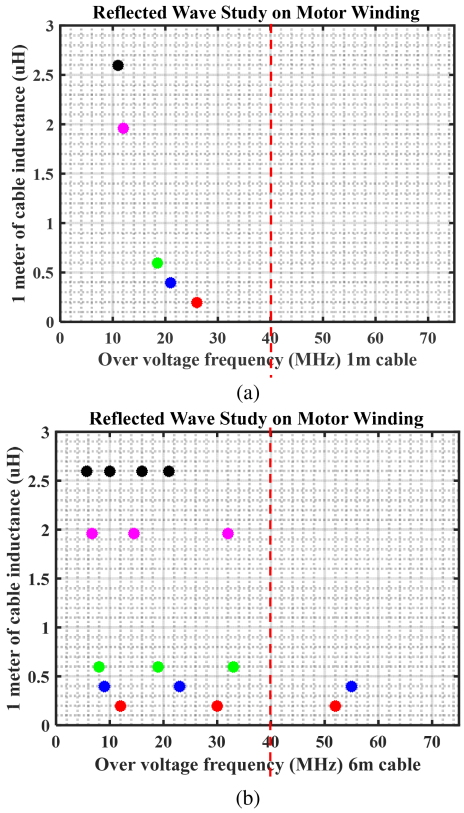

Fig. 13. Variation in ARP occurrence with different cable inductance values.

C. Sensitivity Analysis of ARP Versus Impedance Parameters

Variation in impedance parameters of the cable and load causes the resonance frequency of the OV (cable+ load DM impedance) and load DM AR to shift, which can change the possibility of ARP occurrence. Hence, it is necessary to study the sensitivity of ARP versus each electric parameters.

First, the cable inductance value is varied to study its sensitivity to ARP. Fig. 13 shows the OV resonances versus winding terminal DM AR frequencies using 1 and 6 m cables. The dots show the frequency of the OV resonances with different cable inductance values, while the vertical line at 40 MHz shows the winding terminal DM AR frequency. It can be seen from Fig. 13(a) using 1 m cable for different cable inductance values, the OV resonances are away from winding impedance AR frequency, enough margin from the ARP. So, it would be reliable to use a 1 m cable with the corresponding load and layout. However, using a 6 m cable with a cable inductance of 0.5 uH/m, the third resonance of the OV happens very close to the load AR frequency, as shown in Fig. 13(b). Then, it can pose a risk of insulation failure due to the ARP.

Accordingly, this critical case could be shifted to the cable and motor winding SOA by repositioning the cables to alter the coupling factor, which would impact the overall inductance value. Additionally, conducting a sensitivity study by varying other parasitic elements for a fixed length of cable will provide further insights into the motor drive system. By considering these factors, it is possible to determine the SOA for the motor drive system, as described in the upcoming section.

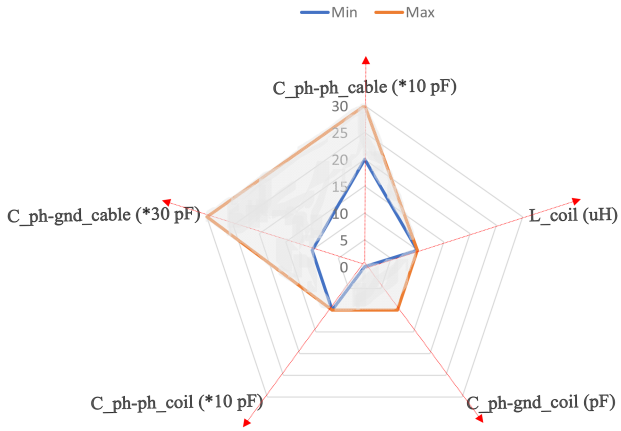

Fig. 14. Cable and motor winding SOA for the system under test using 1 m cable versus HF impedance parameters.

D. Cable and Motor Winding SOA

To maximize the potential of the secure system operation, an SOA is defined for the drive system with respect to converter parameters and operational power ratings in [28] and [29]. However, in this paper, the cable and motor-winding SOA are provided, taking into consideration the interactions between system impedance and ARP. The provided SOA aims to optimize the cabling/ load configuration and electric layout, thereby mitigating the ARP.

To define the SOA, the impact of layout parasitics on the potential shift of the OVs resonance across the load and load DM AR frequencies is considered.

As an example, repeating such a sensitivity study in the previous section on *L_coil* values, it is achieved that the system would be operating in the SOA for *L_coil*< *10 uH,* which directly applied to the SOA chart in Fig. 14. By changing an impedance parameter (e.g., *L_coil*) within the specified range in the gray area, the combination impedance of cable+ load can be controlled. This helps to ensure the OV resonances do not coincide with the load DM AR frequency.

The sensitivity study is conducted varying coil inductance, cable and coil phase-to-ground and phase-to-phase parasitic elements, which leads to the determination of an SOA for the motor drive system shown in Fig. 14. In this figure, *L_coil*, *C_ph_gnd_coil*, *C_ph_ph_coil*, *C_ph_gnd_cable* and *C_ph_ph_cable* indicate coil inductance, phase to ground coil capacitance, phase to phase coil capacitance, phase to ground and phase to phase cable capacitances, respectively. Realizing these relations for the impedance parameters provides an SOA shown in Fig. 14. It should be noted that while varying one impedance parameter, the other parameters are kept constant. This approach allows for a more controlled and systematic investigation of the circuit's response to parameter variations.

The gray area in Fig. 14 is the SOA, which could be a useful tool to determine the change in one of the impedance parameters to shift the operation to SOA in case of ARP occurrence. Factors like the required amount of change, material availability, and practicality can also be considered in the decision-making process.

There would be less freedom to vary the parameters in some applications. For example, the aircraft cabling is less flexible in controlling parasitic capacitances because of fuel line and arcing spacing constraints [30]. If ARP is predicted, the optimization of the $C_{ph\text{-}gnd\_cable}$ to vary the OV resonances would be restricted. However, this would be more practical in industrial applications like motor drives with PV farms.

It is clear from the SOA region that the motor drive system is more sensitive to some of the impedance parameters. So, according to the application, enough accuracy is required to consider these sensitive parameters in the design and layout of the system.

V. Conclusion

This paper describes a guideline to optimize the cabling/ load configuration and electric layout in a motor drive system to mitigate ARP across motor winding insulation. The combination impedance of the cable+ load represents the OV HF resonance frequencies across the load. The investigation on interactions between cable and load HF impedance in different layouts, which causes ARP, is conducted. Then, based on the findings for ARP versus different drive system layouts, a SOA away from the ARP across the load is defined.

It is also learned about the efficacy of the study as:

1) Without sensitivity study, the reliability tests may not ensure a safe operation margin in case of variations in setup as ARP can be highly sensitive to impedance parameter variation.
2) The information on cable and motor winding SOA versus ARP provides an efficient solution compared to secondary solutions like filter design ,which may be required to redesign the filter for different system configurations and layouts. Thus, it can give a, highly dense power system design by eliminating more components.
3) The study reconsiders the general belief on less critical voltage stress in short-cable-connected drives. It is shown that in case of ARP occurrence, the insulation can still be under voltage stress.
4) It is shown that an integrated drive system is bound to ARP occurrence. This should be emphasized as the critical case as the OV was neglected in such systems in the existing literature.
5) The study also shows the importance of mitigating the secondary or low amplitude OVs in case of ARP occurrence.

References

[1] A. I. Emon, Mustafeez-ul-Hassan, A. B. Mirza, J. Kaplun, S. S. Vala, and F. Luo, "A review of high-speed gan power modules: State of the art, challenges, and solutions," *IEEE J. Emerg. Sel. Topics Power Electron.*, vol. 11, no. 3, pp. 2707–2729, Jun. 2023.

[2] Y. Azadeh, A. B. Mirza, K. Choksi, X. Zhang, F. Luo, and K. H. Haran, "dV/dt impact on turn-to-turn overvoltage distribution in motor windings," in *Proc. IEEE Symp. Electromagn. Compat. Signal/Power Integrity*, 2023, pp. 579–584.

[3] J. Zhao, X. Zhang, N. Swaminathan, and K. S. Haran, "An overview of high specific power electrical machines and drives technologies for electrified aircraft," in *Proc. IEEE Energy Convers. Congr. Expo.*, 2022, pp. 1–8.

[4] S. S. Vala, K. Choksi, A. B. Mirza, and F. Luo, "Exploring interactions between reflected wave and partial discharge in WBG motor drives," in *Proc. IEEE Energy Convers. Congr. Expo.*, 2022, pp. 1–5.

[5] A. von Jouanne, P. Enjeti, and W. Gray, "Application issues for PWM adjustable speed AC motor drives," *IEEE Ind. Appl. Mag.*, vol. 2, no. 5, pp. 10–18, Sep./Oct. 1996.

[6] M. J. Scott et al., "Reflected wave phenomenon in motor drive systems using wide bandgap devices," in *Proc. IEEE Workshop Wide Bandgap Power Devices Appl.*, 2014, pp. 164–168.

[7] A. H. Bonnett and G. C. Soukup, "Cause and analysis of stator and rotor failures in three-phase squirrel-cage induction motors," *IEEE Trans. Ind. Appl.*, vol. 28, no. 4, pp. 921–937, Jul./Aug. 1992.

[8] B. Narayanasamy, A. S. Sathyanarayanan, F. Luo, and C. Chen, "Reflected wave phenomenon in SiC motor drives: Consequences, boundaries, and mitigation," *IEEE Trans. Power Electron.*, vol. 35, no. 10, pp. 10629–10642, Oct. 2020.

[9] K. Choksi, Y. Wu, and F. Luo, "Evaluation of factors impacting reflected wave phenomenon in WBG based motor drives," in *Proc. Int. Power Electron. Conf.*, 2022, pp. 736–740.

[10] B. Mirafzal, G. L. Skibinski, and R. M. Tallam, "A failure mode for PWM inverter-fed AC motors due to the antiresonance phenomenon," *IEEE Trans. Ind. Appl.*, vol. 45, no. 5, pp. 1697–1705, Sep./Oct. 2009.

[11] K. Choksi, Y. Wu, M. U. Hassan, F. Luo, B. Liu, and X. Wu, "Inspecting impact of cabling infrastructure on reflected wave and EMI for more electric aircraft (MEA) motor drives," in *Proc. IEEE Transp. Electrific. Conf. Expo*, 2022, pp. 529–533.

[12] M. E. Haque et al., "Design aspects, challenges and benefits of SiC-based integrated switched reluctance machine drives," in *Proc. IEEE Energy Convers. Congr. Expo.*, 2022, pp. 1–5.

[13] S. Sundeep, J. Wang, A. Griffo, and F. Alvarez-Gonzalez, "Antiresonance phenomenon and peak voltage stress within PWM inverter fed stator winding," *IEEE Trans. Ind. Electron.*, vol. 68, no. 12, pp. 11826–11836, Dec. 2021.

[14] Y. Ryu, B.-R. Park, and K. J. Han, "Estimation of high-frequency parameters of AC machine from transmission line model," *IEEE Trans. Magn.*, vol. 51, no. 3, Mar. 2015, Art. no. 8101404.

[15] Z. Chen, D. Boroyevich, P. Mattavelli, and K. Ngo, "A frequency-domain study on the effect of DC-link decoupling capacitors," in *Proc. IEEE Energy Convers. Congr. Expo.*, 2013, pp. 1886–1893.

[16] Y. Xu et al., "Impact of high switching speed and high switching frequency of wide-bandgap motor drives on electric machines," *IEEE Access*, vol. 9, pp. 82866–82880, 2021.

[17] M. T. Fard, J. He, M. Sadoughi, B. Mirafzal, and F. Fateh, "Smart coils for mitigation of motor reflected overvoltage fed by SiC drives," in *Proc. IEEE Appl. Power Electron. Conf. Expo.*, 2023, pp. 1429–1436.

[18] Y. Wu, K. Choksi, M. ul Hassan, and F. Luo, "An extendable and accurate high-frequency modelling of three-phase cable for prediction of reflected wave phenomenon," in *Proc. IEEE Appl. Power Electron. Conf. Expo.*, 2022, pp. 944–950.

[19] O. A. Mohammed, S. Ganu, N. Abed, S. Liu, and Z. Liu, "High frequency PM synchronous motor model determined by FE analysis," *IEEE Trans. Magn.*, vol. 42, no. 4, pp. 1291–1294, Apr. 2006.

[20] P. Brauer, "High-frequency voltage distribution modelling of a slot less PMSM from a machine design perspective," M.S. thesis, EEC Dept., KTH Univ., Stockholm, Sweden, 2018.

[21] T. Jokinen, V. Hrabovcova, and J. Pyrhonen, *Design of Rotating Electrical Machines*. Hoboken, NJ, USA: Wiley, 2013.

[22] Q. Yan, X. Yuan, Y. Geng, A. Charalambous, and X. Wu, "Performance evaluation of split output converters with SiC MOSFETs and SiC Schottky diodes," *IEEE Trans. Power Electron.*, vol. 32, no. 1, pp. 406–422, Jan. 2017.

[23] A. B. Mirza, A. I. Emon, S. S. Vala, and F. Luo, "A comprehensive analysis of current spikes in a split-phase inverter," in *Proc. IEEE Appl. Power Electron. Conf. Expo.*, 2022, pp. 1580–1585.

[24] N. Idir, Y. Weens, and J.-J. Franchaud, "Skin effect and dielectric loss models of power cables," *IEEE Trans. Dielectrics Elect. Insul.*, vol. 16, no. 1, pp. 147–154, Feb. 2009.

[25] L. Zhang, S. Guo, X. Li, Y. Lei, W. Yu, and A. Q. Huang, "Integrated SiC MOSFET module with ultra-low parasitic inductance for noise free ultra-high speed switching," in *Proc. IEEE 3rd Workshop Wide Bandgap Power Devices Appl.*, 2015, pp. 224–229.

[26] S. Wang, K. Pengju, and F. C. Lee, "Common mode noise reduction for boost converters using general balance technique," *IEEE Trans. Power Electron.*, vol. 22, no. 4, pp. 1410–1416, Jul. 2007.

[27] M. D. Hennen, M. Niessen, C. Heyers, H. J. Brauer, and R. W. De Doncker, "Development and control of an integrated and distributed inverter for a fault tolerant five-phase switched reluctance traction motor," *IEEE Trans. Power Electron.*, vol. 27, no. 2, pp. 547–554, Feb. 2012.
[28] Z. Zhengming, L. Yuan, H. Bai, and T. Lu, "System safe operation area based on switching characteristics," *Electromagn. Transients Power Electron. Syst.*, 2019, pp. 199–242. [Online]. Available: https://link.springer.com/chapter/10.1007/978-981-10-8812-4_5
[29] T. Hossen, F. Fateh, F. Sadeque, and B. Mirafzal, "Projection of safe operation for inverters using artificial intelligence-based stability criterion," in *Proc. IEEE Appl. Power Electron. Conf. Expo.*, 2023, pp. 3083–3088.
[30] "Aircraft electrical wiring interconnect system (EWIS) best practices," FAA, USA. [Online]. Available: https://peda.net/ksao/oppimisymp%C3%A4rist%C3%B6/koulutusalat/tjla/alv/lentokoneasentaja/lph/m7hjkl/7se/tukimateriaali/7et:file/download/92bb21d1448d71ddae13fb3274240d7-6cb5b17d3/7.7%20EWIS%20Tukimateriaali.pdf

Yalda Azadeh (Graduate Student Member, IEEE) is currently working toward the Ph.D. degree in electrical engineering—power electronics from Stony Brook University, Stony Brook, NY, USA.

She is currently a Graduate Research Assistant and involved in research projects with the Oak Ridge National Laboratory and Federal Aviation Administration. In 2022, she was a research intern at On-Semiconductor, Phoenix, AZ, USA. Her research interests include but are not limited to Power Electronics, EMC/ EMI, WBG-based motor drive systems and MVDC breakers using WBG-based power electronics.

Kushan Choksi (Graduate Student Member, IEEE) is currently working toward the Ph.D. degree in electrical engineering—power electronics from Stony Brook University, Stony Brook, NY, USA.

He has two years of research experience at Indian Institute of Technology, Gandhinagar (2017–2018) and Indian Institute of Technology, Bombay (2018–2019) as Research Project Manager. His research interest includes development of control algorithms for power hardware in loop (P-Hil) and digital twin of power electronic systems. He is also interested in design and study EMI models of dc–ac and dc–dc converters using modern WBG devices.

Abdul Basit Mirza (Graduate Student Member, IEEE) received the bachelor's degree (Hons.) in electrical engineering (power) from the University of Engineering and Technology, Lahore, Pakistan, in 2018, and the master's degree in 2022 from Stony Brook University, Stony Brook, NY, USA with a concentration in MVDC breakers using WBG-based power electronics. He is currently working toward the Ph.D. degree in electrical engineering from Stony Brook University.

He is a Graduate Research Assistant and involved in research projects with the Oak Ridge National Laboratory and Federal Aviation Administration. In 2022, he was a research intern at GE Global Research, Niskayuna, NY, USA. His research interests include system level design of high-density WBG-based power converters and electromagnetic interference and compatibility (EMI/EMC) characterization.

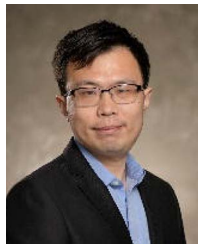

Xiaolong Zhang (Member, IEEE) was born in Hunan, China. He received the bachelor's and master's degrees in electrical engineering from the Huazhong University of Science and Technology (HUST), Wuhan, China, in 2011 and 2014, respectively. He received the Ph.D. degree in electrical and computer engineering from the University of Illinois Urbana-Champaign, Champaign, IL, USA, in 2022.

From 2014 to 2015, he was working as a Research Engineer in the Nanyang Technological University (NTU), Singapore. He is currently working as a Postdoctoral Researcher from the University of Illinois Urbana-Champaign. His research interests include electric machine design, motor drives and control, and electrified transportation systems.

Yuxuan Wu (Graduate Student Member, IEEE) received the B.E. degree in electrical engineering from Stony Brook University, Stony Brook, NY, USA, in 2020. He is working toward the Ph.D. degree from Stony Brook University, specializing in power electronics.

His research focuses on designing and applying high-power-density power modules using WBG devices, low and medium-voltage power conversion systems, cable and converter modeling, and EMI/EMC analysis. As a Graduate Research Assistant, he is actively involved in a project funded by the Office of Naval Research. Additionally, he gained industry experience as an Intern at GE Global Research (Aerospace) in Niskayuna, NY, during the summer of 2023. His internship focused on conducting an EMI/EMC study for more electric aircraft.

Fang Luo (Senior Member, IEEE) received the bachelor's and Ph.D. degrees from the Huazhong University of Science and Technology, Wuhan, China, and jointly from Virginia Tech, Blacksburg, VA, USA, in 2003 and 2010, respectively.

He was an Assistant Professor with the Electrical Engineering Department, University of Arkansas, Fayetteville, AR, USA, from 2017 to 2020, and a Research Assistant Professor with The Ohio State University, Columbus, OH, USA, from 2014 to 2017. He was a Visiting Ph.D. Student from 2007 to 2010 and then a Postdoctoral Researcher from 2010 to 2014 with Virginia Tech. He is currently an Empire Innovation Associate Professor and the Director of the Spellman High Voltage Laboratory, Stony Brook University (SUNY Stony Brook), Stony Brook, NY, USA, with his background in power electronics. His research interests include high-power density converter design, high-density electromagnetic interference filter design and integration, and power module packaging/integration for WBG devices.

Dr. Luo is a Member of the American Institute of Aeronautics and Astronautics (AIAA) and American Society of Mechanical Engineers (ASME). He was the recipient of the NSF CAREER Award.

Kiruba S. Haran (Fellow, IEEE) received the B.Sc. degree in electronic and electrical engineering from Obafemi Awolowo University (OAU), Ile-Ife, Nigeria, in 1994, and the Ph.D. degree in electric power engineering from the Rensselaer Polytechnic Institute (RPI), Troy, NY, USA, in 2000.

He spent 13 years with GE Research, Niskayuna, NY, USA, as a Senior Engineer and the Manager of the Electrical Machines Laboratory. He is currently a Professor of electrical and computer engineering and the Director of the Grainger Center for Electric Machinery and Electromechanics, University of Illinois at Urbana–Champaign, Urbana, IL, USA. His current research interests include high-specific power electrical machines and drives, with both superconducting and noncryogenic approaches.